

Atmospheric CO₂ decline during the Pliocene intensification of Northern Hemisphere glaciations

Gretta Bartoli,¹ Bärbel Hönisch,² and Richard E. Zeebe³

Received 8 September 2010; revised 6 September 2011; accepted 9 September 2011; published 16 November 2011.

[1] Several hypotheses have been put forward to explain the onset of intensive glaciations on Greenland, Scandinavia, and North America during the Pliocene epoch between 3.6 and 2.7 million years ago (Ma). A decrease in atmospheric CO₂ may have played a role during the onset of glaciations, but other tectonic and oceanic events occurring at the same time may have played a part as well. Here we present detailed atmospheric CO₂ estimates from boron isotopes in planktic foraminifer shells spanning 4.6–2.0 Ma. Maximal Pliocene atmospheric CO₂ estimates gradually declined from values around 410 μatm to early Pleistocene values of 300 μatm at 2.0 Ma. After the onset of large-scale ice sheets in the Northern Hemisphere, maximal $p\text{CO}_2$ estimates were still at 2.5 Ma +90 μatm higher than values characteristic of the early Pleistocene interglacials. By contrast, Pliocene minimal atmospheric CO₂ gradually decreased from 310 to 245 μatm at 3.2 Ma, coinciding with the start of transient glaciations on Greenland. Values characteristic of early Pleistocene glacial atmospheric CO₂ of 200 μatm were abruptly reached after 2.7 Ma during the late Pliocene transition. This trend is consistent with the suggestion that ocean stratification and iron fertilization increased after 2.7 Ma in the North Pacific and Southern Ocean and may have led to increased glacial CO₂ storage in the oceanic abyss after 2.7 Ma onward.

Citation: Bartoli, G., B. Hönisch, and R. E. Zeebe (2011), Atmospheric CO₂ decline during the Pliocene intensification of Northern Hemisphere glaciations, *Paleoceanography*, 26, PA4213, doi:10.1029/2010PA002055.

1. Introduction

[2] To better understand and constrain future climate change in a high-CO₂ world, it is essential to study potential CO₂ analogs in Earth's history and the climate at that time. The Pliocene epoch (5.33–2.6 Ma) prior to the intensification of Northern Hemisphere glaciation at about 2.75 Ma is a likely candidate for such a high-CO₂ analog. With a similar land-ocean configuration as today, Pliocene climate prior to 3.0 Ma was on average 3°C warmer than today with smaller terrestrial and sea ice extent [Haywood and Valdes, 2004, and references therein] and a partially deglaciated West Antarctic Ice Sheet [Naish *et al.*, 2009]. Greenland and North Canada were forested, with possible small glacier outlets and terrestrial summer temperatures between 5 and 4 Ma were 14°C warmer than today [Ballantyne *et al.*, 2006]. Accumulating evidence suggests that Pliocene CO₂ levels prior to 3.0 Ma were higher than the preindustrial level of 280 μatm [Seki *et al.*, 2010; Pagani *et al.*, 2010] and possibly close to today's level of 392 μatm (P. Tans and

R. Keeling, NOAA ESRL, www.esrl.noaa.gov/gmd/ccgg/trends/).

[3] To explain the onset of Northern Hemisphere glaciations between 3.6 and 3.0 Ma [Mudelsee and Raymo, 2005] and its intensification about 2.75 Ma onward [Haug *et al.*, 2005], several mechanisms have been put forward. In a previous modeling study, a linear decrease in CO₂ from high Pliocene concentrations to Pleistocene concentrations triggers large-scale ice sheets on the Northern Hemisphere after 2.9–2.7 Ma when obliquity was lowest (i.e., low summer insolation) [Li *et al.*, 1998]. A recent modeling study compared the respective effects of the closure of Panamanian seaways, the end of a permanent El Niño state in the equatorial Pacific, and the tectonic uplift of the Rocky Mountains on the size of the Greenland ice sheet [Lunt *et al.*, 2008, and references therein]. This comparison suggested that a decrease in atmospheric CO₂ from a Pliocene level of 400 μatm to the preindustrial maximum of 280 μatm is most likely the culprit causing the onset of permanent Northern Hemisphere glaciations [Lunt *et al.*, 2008]. A Northern Hemisphere glaciation threshold of 280 μatm CO₂ has also been suggested by DeConto *et al.* [2008], and Seki *et al.* [2010] presented evidence for CO₂ dropping from 330 to 400 μatm to ~280 μatm between 3.2 and 2.8 Ma, thus confirming the coincidence between CO₂ decrease and Northern Hemisphere glaciations.

[4] However, the reasons for the decrease in atmospheric CO₂ have not yet been determined. Moreover, a decrease in

¹Geological Institute, ETH Zurich, Zurich, Switzerland.

²Lamont-Doherty Earth Observatory, Earth Institute at Columbia University, Palisades, New York, USA.

³Department of Oceanography, School of Ocean and Earth Science and Technology, University of Hawai'i at Mānoa, Honolulu, Hawaii, USA.

atmospheric CO₂ may not be the only prerequisite to the persistence of ice sheets on the Northern Hemisphere. Two studies recently proposed that the permanent El Niño state characterizing the early Pliocene equatorial Pacific would have prevented the growth of ice sheets at various locations on the Northern Hemisphere prior to 2.75–3.0 Ma [Huybers and Molnar, 2007; Vizcaino et al., 2010]. Therefore it is necessary to determine the exact timing of CO₂ changes, so that the tectonic and biogeochemical mechanisms of climate change and their causal relations can be better understood.

[5] In this study, we attempt to answer these questions by reconstructing changes in the partial pressure of carbon dioxide ($p\text{CO}_2$) in surface seawater over the time period 4.6 to 2.0 Ma from planktic foraminiferal boron isotope ratios. Building on earlier work [Hemming and Hanson, 1992], boron isotope ratios recorded in planktic foraminifer shells have been applied successfully to reconstruct changes in surface seawater pH and aqueous $p\text{CO}_2$ over the Pleistocene [Foster, 2008; Hönisch and Hemming, 2005; Hönisch et al., 2009]. Boron isotopes in marine carbonates are a function of seawater pH, since the relative abundance and isotopic composition of the two dominant dissolved boron species in seawater, i.e., boric acid and borate, change with pH. The charged borate is preferentially incorporated into marine carbonates so that their recorded boron isotopic composition ($\delta^{11}\text{B}$) increases with seawater pH [Hemming and Hanson, 1992].

[6] To understand how the uncertainties related to the reconstructions of paleoenvironmental proxies for the Pliocene epoch influence the reconstruction of $p\text{CO}_2$, we also performed a sensitivity study of $p\text{CO}_2$ estimates to the uncertainties on sea surface temperature (SST) related to uncertainties on the evolution of the seawater Mg/Ca ratio (Mg/Ca_{s.w.}), and the seawater boron isotope ratio ($\delta^{11}\text{B}_{\text{s.w.}}$) used to calculate $p\text{CO}_2$ from boron isotope estimates.

2. Material and Methods

2.1. Site Location

[7] Estimating atmospheric CO₂ from marine proxy records requires a location where aqueous and atmospheric CO₂ are in close equilibrium. We have selected ODP site 999, located in the Columbian Basin (12°N, 78°W, 2839 m water depth) in the Caribbean Sea, which has previously been studied by Seki et al. [2010], albeit in lower resolution. Modern surface water is slightly oversaturated with respect to CO₂ ($\pm 17 \mu\text{atm}$) and Caribbean waters therefore act as a minor annual source of CO₂ to the atmosphere [Takahashi et al., 2007]. A boron isotope study covering the last 140 ky suggests that glacial/interglacial atmospheric CO₂ amplitudes can be captured from this site [Foster, 2008], suggesting that the strength of the CO₂ source did not change significantly during Pleistocene glacial/interglacial cycles.

[8] Potential changes in sea-air equilibrium during the Pliocene may include upwelling of nutrient-rich and CO₂-rich intermediate water at site 999, and enhanced surface water productivity. Some authors have suggested that Pacific waters rich in upwelled CO₂ would have entered the Caribbean Sea prior to the final closure of the Panama seaway, elevating surface $p\text{CO}_2$ at site 999 as compared to the atmosphere [Seki et al., 2010]. The inflow of Pacific water into the Caribbean can be monitored by comparison with site

1241 in the equatorial Pacific [Bartoli et al., 2005; Steph et al., 2006, 2010]. Seki et al. [2010] calculated $p\text{CO}_2$ values at sites 1241 and 999 from alkenone ε_p estimates and found higher $p\text{CO}_2$ on the Pacific side of the Isthmus as compared to the Caribbean side for the last 4.5 My. The authors implied that prior to the closure of Panama at 3.5 Ma upwelled CO₂-rich surface waters entered the Caribbean Sea and rendered site 999 a minor source of CO₂ to the atmosphere. However, the raw ε_p values and trends at sites 1241 and 999 are actually similar, and do not indicate any coincident change with the final closure of Panama at 3.5 Ma or later. There is therefore no direct proxy evidence that the Pacific surface inflow into the Caribbean increased Caribbean $p\text{CO}_2$ prior to 3.5 Ma.

[9] In addition, the Pacific surface waters entering the Caribbean Sea through the Panamanian seaways, and monitored at site 1241, most likely derived from the North Equatorial Countercurrent, which originates in the oligotrophic West Pacific Warm Pool [Steph et al., 2010]. A study of changes in the thermocline depth at site 1241 based on Mg/Ca measured on the thermocline dwelling *Globorotalia tumida* shows no upwelling conditions between 5.5 and 2.0 Ma [Steph et al., 2010]. Upwelling did occur along the Peruvian coast, monitored at site 1243, and intensified after 3.9 Ma but never reached site 1241 [Steph et al., 2010]. The evolution of surface water stratification at site 999 is monitored by Mg/Ca-based SST from the surface dwelling *Globigerinoides sacculifer* and the thermocline dwelling *Neogloboquadrina dutertrei* [Steph et al., 2006, 2010]. They show a deepening of the thermocline following the closure of Panama between 4.8 and 4.0 Ma but constant surface water stratification conditions thereafter [Steph et al., 2006, 2010]. Similarly, the $\delta^{13}\text{C}$ record of *G. sacculifer* at site 999 [Haug et al., 2001, unpublished data, 1999] does not show any significant changes between 5.0 and 2.0 Ma, leading us to believe that there were no major changes in surface productivity or nutrient supply that would characterize upwelling conditions. Finally, a study of Caribbean mean annual temperature range off the Panamanian coasts based on the size of bryozoan zooids suggests that coastal upwelling in the southern Caribbean Sea stopped after the closure of Panama between 4.25 and 3.45 Ma [O'Dea et al., 2007], although it is not sure whether these upwelled waters would have reached offshore site 999 prior to the closure. There is no absolute certainty that surface waters at site 999 were always in CO₂ equilibrium with the atmosphere during the Pliocene. However, based on the evidence described above, we assume that surface waters were close to equilibrium with the atmosphere at least from 3.45 Ma onward, and that there is little evidence for upwelling between 3.45 and 4.6 Ma.

2.2. Boron Isotope Analysis

[10] Our aqueous $p\text{CO}_2$ estimates are based on boron isotope ratios ($^{11}\text{B}/^{10}\text{B}$) in shells of the planktic foraminifer *G. sacculifer*. Hönisch and Hemming [2004] observed that shells $>425 \mu\text{m}$ in diameter record surface seawater pH. Although several studies have observed a dissolution effect on smaller individuals [Hönisch and Hemming, 2004; Ni et al., 2007], the largest shell size classes of *G. sacculifer* are most resistant to dissolution, and their boron isotopic composition records surface seawater pH variations [Hönisch and Hemming, 2004; Ni et al., 2007]. Sediment samples were

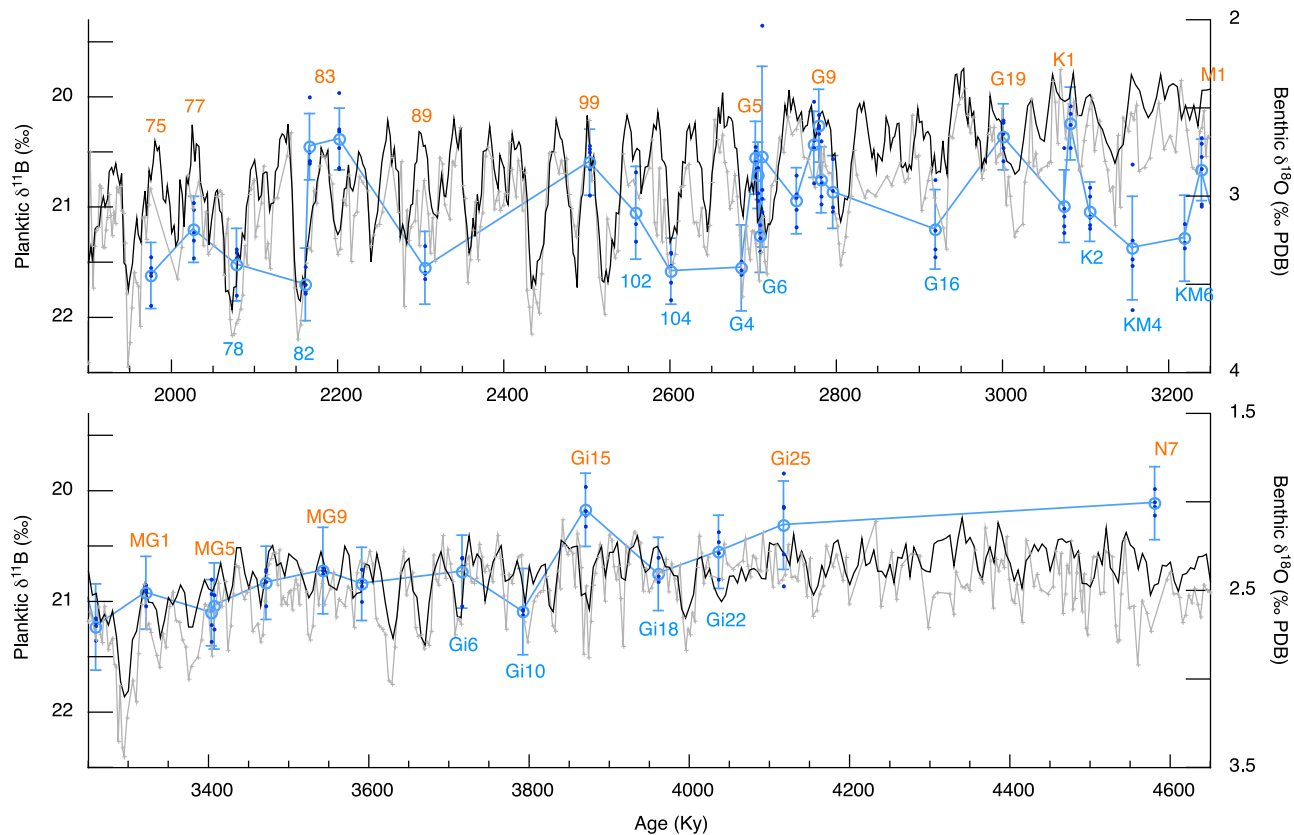


Figure 1. Planktic foraminiferal $\delta^{11}\text{B}$ and benthic foraminiferal $\delta^{18}\text{O}$ records. Repeat boron isotope analyses of individual sample solutions are indicated by dark blue dots, average values are shown in light blue, and uncertainties reflect internal or external 2 standard error reproducibility, whichever is larger. Grey crosses depict benthic foraminiferal $\delta^{18}\text{O}$ at site 999 measured on *C. wuellerstorfi* [Haug and Tiedemann, 1998]. The black line shows the benthic foraminiferal $\delta^{18}\text{O}$ stack LR04 [Lisiecki and Raymo, 2005], which reflects changes in deep ocean temperature and global ice volume. Glacial (blue) and interglacial (orange) MIS used for the descriptions of amplitudes are labeled according to the nomenclature by Lisiecki and Raymo [2005]. Note the right y axis change of scale from top to bottom.

selected according to glacial and interglacial extremes in the benthic oxygen isotope stratigraphy of ODP 999A. Prior to washing the sediment, the first set of samples prepared at ETH Zürich was soaked for a brief period (no more than 2–3 h) in 3% H_2O_2 to help disaggregate the sediment (Data Set S1 in the auxiliary material).¹ The second set of samples prepared at LDEO was freeze-dried (Data Set S1). Samples were then washed through a 63 μm sieve and then oven dried. Between 30 and 80 specimens with a total sample weight of 1–4 mg were analyzed.

[11] Shells were cracked between two glass slides, bleached overnight with 5% NaOCl to remove organic matter, and then rinsed 10 times with quartz distilled water under repeated ultrasonication and centrifugation steps. Mechanical cleaning by ultrasonication efficiently removes adherent clay particles [Martin and Lea, 2002; Deyhle and Kopf, 2004], which could be a source of B contamination. Samples were dissolved with 2N quartz-distilled HCl and aliquots containing ~ 1 ng B were loaded onto outgassed zone

refined Re filaments. 1 μl of boron-free seawater was added to each aliquot to facilitate ionization and discourage fractionation. Boron isotopes were then measured as BO_2^- ions on a Thermo Scientific TRITON thermal ionization mass spectrometer (TIMS) at the Lamont-Doherty Earth Observatory (LDEO). Analyses were done at a filament temperature of 980°C and a minimum of 3 acceptable analyses were collected of each sample solution to eliminate analytical artifacts such as excessive fractionation ($>1\%$ over the 20–30 min of data acquisition) and/or isobaric interference on mass 42 ($>5,000$ counts on mass 26) by organic matter contamination. $\delta^{11}\text{B}$ was normalized to NIST 951 boric acid standard, similarly loaded with boron-free seawater and measured at 980°C. Three out of a total 195 analyses were excluded as analytical outliers because their isotope ratio deviated by >2 sd from the population mean of all acceptable analyses (Chauvenet's criterion) collected on the respective samples (Data Set S1 and Figure S1). Because each sample solution is homogenous, such a deviating analysis was rejected as an outlier. The analytical uncertainty reported on our analyses (Figure 1) is the 2σ standard error (2 standard errors = $2 \text{ sd}/\sqrt{N}$), which takes into account the number of acceptable analyses ($N = 3\text{--}7$) for each sample and the

¹Auxiliary material data sets are available at <ftp://ftp.agu.org/apend/pa/2010pa002055>. Other auxiliary material files are in the HTML. doi:10.1029/2010PA002055.

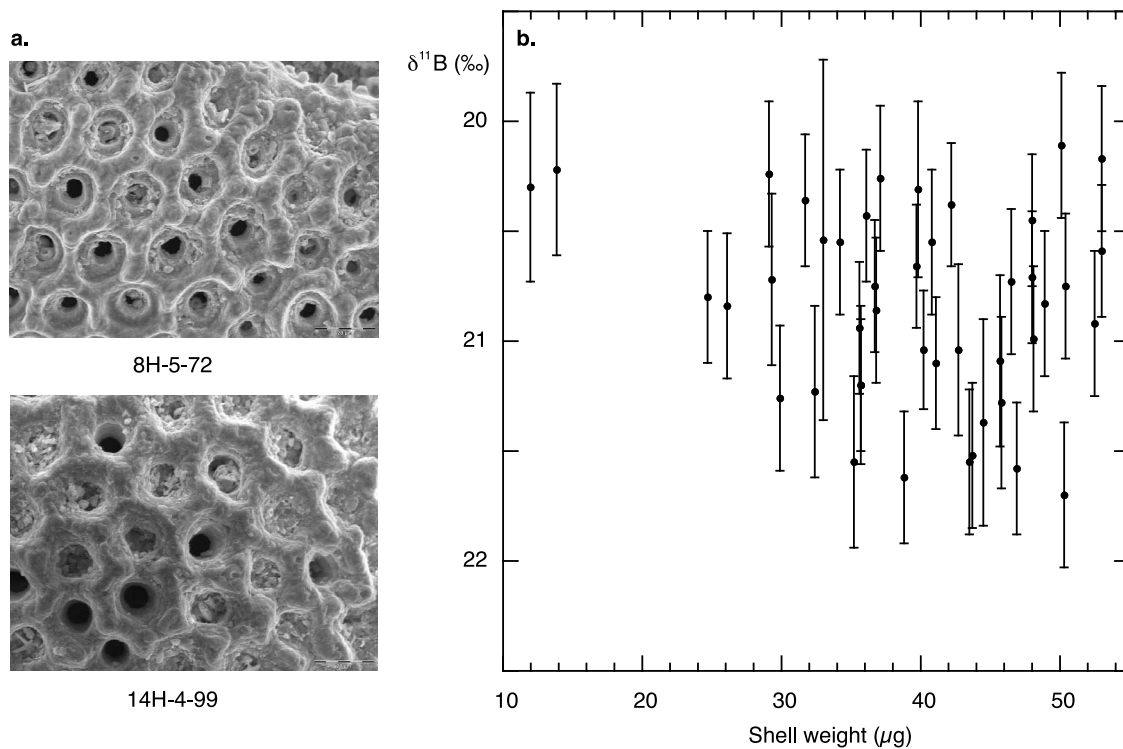


Figure 2. (a) SEM photos of the shell surface of two uncleaned *G. sacculifer* specimens taken from samples dated at (top) 2.16 Ma and (bottom) 4.03 Ma. Shells show no obvious sign of dissolution such as widened pore funnels or fissures. See also Data Set S1 for additional images. (b) Planktic foraminiferal $\delta^{11}\text{B}$ with analytical error bars versus foraminiferal shell weight measured after cleaning. No correlation between shell weight and $\delta^{11}\text{B}$ values confirms that the picked foraminifer shells used for $\delta^{11}\text{B}$ analysis are unlikely to be biased by dissolution.

reproducibility of the NBS 951 boric acid standard (2 standard errors = 0.09‰) or, if higher, the 2 standard error external error of an in-house carbonate standard routinely analyzed at LDEO. The uncertainty of repeat data analysis is generally better than 0.34‰ (Figure 1).

[12] The $\delta^{11}\text{B}$ data measured on the Thermo Scientific TRITON are lighter in comparison to data measured on the NBS design TIMS at SUNY Stony Brook [Hönisch and Hemming, 2004, 2005]. An interlaboratory comparison of modern and fossil *G. sacculifer* samples measured at LDEO on the TRITON and at SUNY Stony Brook on the NBS instrument, revealed a consistent offset of -1.1‰ ($\pm 0.19\text{‰}$) on the TRITON that is not accounted for by standardization against NIST 951 [Hönisch et al., 2009]. The only difference other than the instrument is the use of boron free seawater at LDEO, which was added to both, samples and the boric acid standard. We do not know what causes this difference but we found that poor ionization at 980°C and excessive fractionation at temperatures $>1020^\circ\text{C}$ prohibit the analysis of foraminifer samples without boron free seawater on the TRITON. This instrument offset affects the absolute value but not the relative difference between glacial and interglacial samples, which allows for straightforward translation of boron isotope values into pH estimates [Hönisch et al., 2009].

2.3. Evaluation of Dissolution Bias and Reproducibility

[13] Although site 999 is characterized by excellent carbonate preservation after 4.6 Ma [Haug and Tiedemann, 1998], boron isotopes in planktic foraminifer shells are believed to be prone to partial shell dissolution [Hönisch and Hemming, 2004] and it is imperative to exclude potential dissolution bias on the measured $\delta^{11}\text{B}$. We therefore took Scanning Electron Microscopy images of individual shells randomly selected from the samples (Figure 2a and Data Set S1). SEM images do not show any dissolution artifact and show a pristine gametogenic calcite layer, which is typical for well-preserved specimens [Hönisch and Hemming, 2004]. We also compared measured $\delta^{11}\text{B}$ with the shell weight of analyzed foraminifers (Figure 2b and Data Set S1). Dissolution would lower the foraminifers' shell weight and decrease the measured $\delta^{11}\text{B}$, although other factors may also modify the initial foraminifer shell weight such as the carbonate ion concentration at the time of shell formation. No systematic correlation between low shell weight and low measured $\delta^{11}\text{B}$ was observed (Figure 2b). Two samples at 4.2 and 2.2 Ma yielded out-of-range $\delta^{11}\text{B}$ values that could not be replicated by additionally picked foraminifer shells from the same samples (Data Set S1). The samples were depleted in large shells after these analyses and without additional confirmation data from these two samples were not interpreted further. Such poor reproducibility is unusual, as can be inferred from comparison of

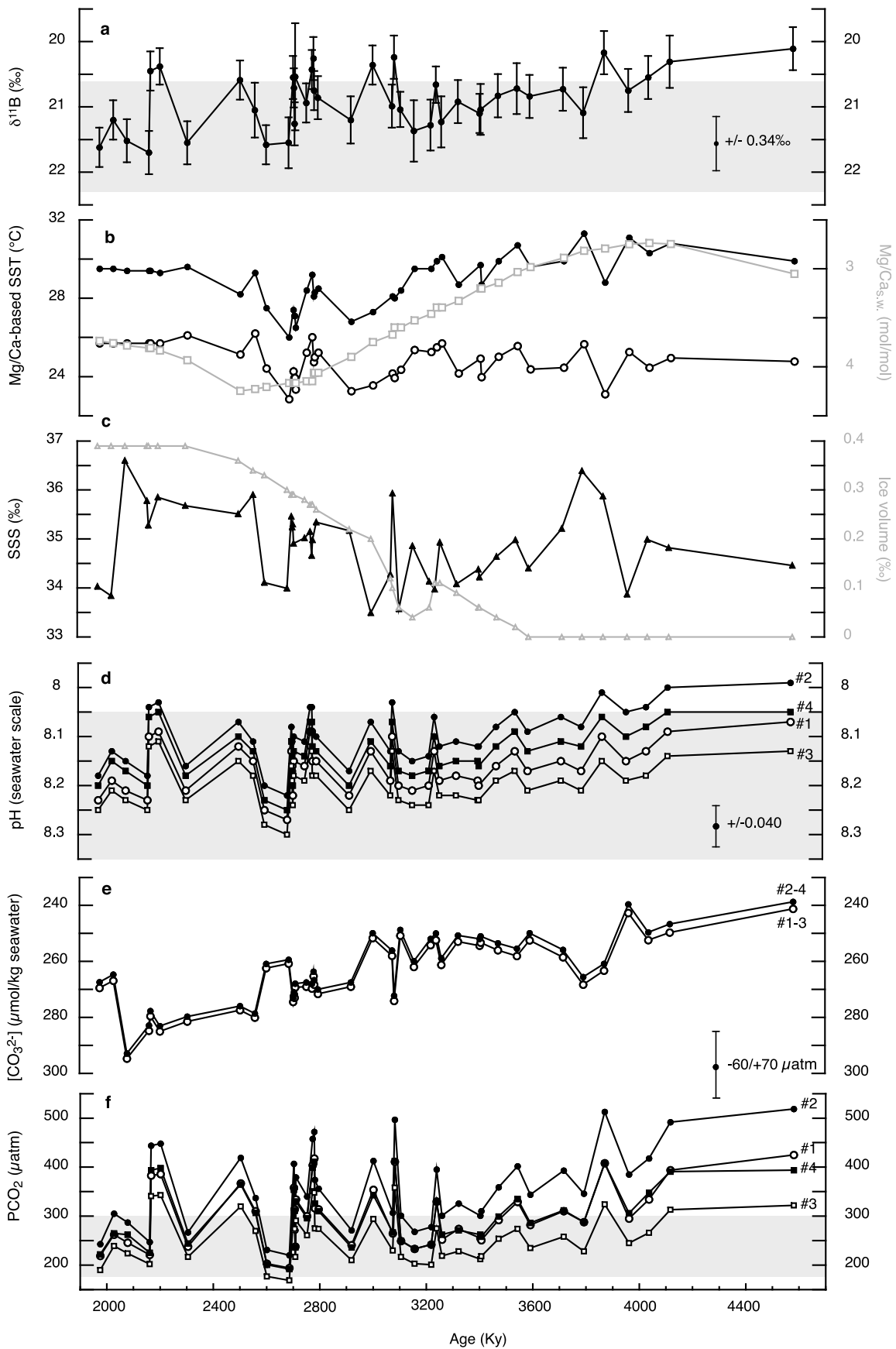


Figure 3

three shell-size specific sample pairs that reproduce within $\pm 0.13\%$ (Data Set S1).

2.4. Seawater pH and Aqueous $p\text{CO}_2$ Calculations

2.4.1. Calculations of pH

[14] To reconstruct seawater pH and aqueous $p\text{CO}_2$ from $\delta^{11}\text{B}$ (Figure 3a), a number of parameters are necessary that are summarized in Figures 3b, 3c, and 3e. To calculate pH (Figure 3d), species-specific empirical calibration curves are applied, which consistently show a shallower $\delta^{11}\text{B}/\text{pH}$ slope than suggested for dissolved borate in seawater [Klochko *et al.*, 2006]. Therefore instead of using an aqueous fractionation factor that does not describe the empirical pH dependence of our measured $\delta^{11}\text{B}$ data, we apply the species-specific empirical calibration curves established by NTIMS analysis. To reflect the difference between the aqueous fractionation $\varepsilon = 27.2\%$ and the value that best describes the empirical data, we distinguish the use of the empirical value as $\varepsilon^* = 19.4\%$ at 25°C and atmospheric pressure. The corresponding fractionation factor α^* can then be calculated as $\alpha^* = \varepsilon^*/1000 + 1$. To translate our measured boron isotope data into pH values, we used equation (1) after Hönlisch *et al.* [2007]:

$$\text{pH} = \text{pK}_B - \log\left(-(\delta^{11}\text{B}_{\text{s.w.}} - \delta^{11}\text{B}_c - a) / (\delta^{11}\text{B}_{\text{s.w.}} - \alpha^* \times (\delta^{11}\text{B}_c + a) - \varepsilon^*), \quad (1)$$

where pK_B is the equilibrium constant for the boric acid/borate system [Dickson, 1990], $\delta^{11}\text{B}_{\text{s.w.}}$ is the $\delta^{11}\text{B}$ value of seawater, $\delta^{11}\text{B}_c$ is the isotopic composition of the measured carbonate, and ‘ a ’ = -4.2% is the constant offset between the apparent borate and empirical $\delta^{11}\text{B}/\text{pH}$ calibration curve for *G. sacculifer*, adjusted for the additional instrumental difference described above [Sanyal *et al.*, 2001; Hönlisch *et al.*, 2009].

2.4.2. Uncertainties of Seawater $\delta^{11}\text{B}$

[15] The present-day value of $\delta^{11}\text{B}_{\text{s.w.}}$ has recently been estimated to $\sim 39.61\%$ [Foster *et al.*, 2010] but modeling studies [Lemarchand *et al.*, 2000; Simon *et al.*, 2006] suggest it was different during the Pliocene, despite the residence time of B in the ocean being about 14 My [Spivack and Edmond, 1987]. Indeed, $\delta^{11}\text{B}_{\text{s.w.}}$ can be modified by a number of sources and sinks and Lemarchand *et al.* [2000] estimated a secular decrease of $\sim 0.1\%/My$ from 0 to 20 Ma,

i.e., $\delta^{11}\text{B}_{\text{s.w.}} \cong 39\%$ at 5 Ma. Similarly, Simon *et al.* [2006] estimated the $\delta^{11}\text{B}$ ratio of the oceanic crust and performed a sensitivity study on $\delta^{11}\text{B}_{\text{s.w.}}$, considering various exchange rates between the oceanic crust and the ocean. Their data, excluding variations in riverine input as studied by Lemarchand *et al.* [2000, 2002], show a decrease in $\delta^{11}\text{B}_{\text{s.w.}}$ from the present-day value to 34–38‰ at 5 Ma. Similarly, Pearson and Palmer [1999] developed a $\delta^{11}\text{B}_{\text{s.w.}}$ model based on the water column pH profile estimated from various deep-dwelling planktic foraminifer species, which has then been used by Pearson and Palmer [2000] to estimate Cenozoic $p\text{CO}_2$. These estimates are uncertain because Pearson and Palmer [1999] have not considered the potential vital effects in different foraminifer species. However, despite any reservation to the accuracy of their estimate, their values yield intermediate $\delta^{11}\text{B}_{\text{s.w.}}$ estimates of 38.6–39‰ for the period 6–3.9 Ma. A recent estimation of $\delta^{11}\text{B}_{\text{s.w.}}$ from Messinian marine halite yield a much lower value of 34.65‰ ($\pm 0.3\%$) at 5.5 Ma [Paris *et al.*, 2010]. Such low $\delta^{11}\text{B}_{\text{s.w.}}$ would imply Pliocene surface seawater $\text{pH} > 8.5$, and in turn would decrease $\delta^{11}\text{B}$ -based Pliocene atmospheric $p\text{CO}_2$ (in this study and for data by Seki *et al.* [2010]) to levels lower than Pleistocene level. Such an estimate seems inconsistent with warmer climate at that time. Because uncertainties in all these estimates are large, we chose to adopt Lemarchand’s estimate of $\delta^{11}\text{B}_{\text{s.w.}}$, which suggests a decrease of $0.1\%/My$ from today’s value. For our pH reconstruction we thus consider two cases with (1) constant $\delta^{11}\text{B}_{\text{s.w.}}$ of 39.61‰ and (2) $\delta^{11}\text{B}_{\text{s.w.}}$ decreasing from today’s value of 39.61‰ to 39.15‰ at 4.6 Ma. Due to the slow rate of change in the processes that govern the oceanic boron budget, short-term changes in $\delta^{11}\text{B}_{\text{s.w.}}$ are not to be expected [Lemarchand *et al.*, 2002].

2.4.3. Uncertainties of Sea Surface Temperature Reconstructions

[16] The calculation of pK_B requires knowledge of sea surface temperature (SST), sea surface salinity (SSS) and water pressure. Pliocene SST was reconstructed from Mg/Ca measured on *G. sacculifer* (315–400 μm) at site 999 by Groeneveld [2005]. The incorporation of Mg in foraminifer shells during calcification mainly depends on the temperature of the seawater in which they grow, but also on the Mg/Ca ratio of the growth medium [Delaney *et al.*, 1985]. Pliocene variations in seawater Mg/Ca ($\text{Mg}/\text{Ca}_{\text{s.w.}}$) may not be

Figure 3. Parameters used to reconstruct seawater pH and $p\text{CO}_2$ at ODP site 999. (a) ratios of $\delta^{11}\text{B}$ measured on *G. sacculifer* (425–500 μm) with analytical error bars. Grey shading indicates Pleistocene minimal and maximal values obtained via the same method on *G. sacculifer* at site 668B [Hönlisch *et al.*, 2009], corrected for the 1.1‰ offset between the two laboratories (see text). (b) SST obtained from Mg/Ca ratios measured on *G. sacculifer* (315–400 μm) at site 999 [Groeneveld, 2005] (open dots), $\text{Mg}/\text{Ca}_{\text{s.w.}}$ (open squares), and SST adjusted to secular changes in $\text{Mg}/\text{Ca}_{\text{s.w.}}$ (solid dots). [Fantle and DePaolo, 2005, 2006] using the procedure outlined by Medina-Elizalde *et al.* [2008]. (c) SSS reconstructed from $\delta^{18}\text{O}_{\text{s.w.}}$ (solid triangles; see text) and from the record of ice volume change in open triangles [Mudelsee and Raymo, 2005]. (d) Surface water pH reconstructions according to the four scenarios defined in the text: 1, unadjusted SST and modern $\delta^{11}\text{B}_{\text{s.w.}}$; 2, adjusted SST and modern $\delta^{11}\text{B}_{\text{s.w.}}$; 3, unadjusted SST and Pliocene $\delta^{11}\text{B}_{\text{s.w.}}$; and 4, adjusted SST and Pliocene $\delta^{11}\text{B}_{\text{s.w.}}$. Grey shading indicates Pleistocene maximal and minimal pH values [Hönlisch *et al.*, 2009]. Average error bar is indicated. (e) Carbonate ion concentration ($[\text{CO}_3^{2-}]$) estimated from past variations in the global CCD and in $[\text{Ca}^{2+}]$, using SSS in Figure 3c and adjusted SST (solid dots) and unadjusted SST (open dots) in Figure 3b. (f) Surface seawater $p\text{CO}_2$ reconstructions according to the four scenarios defined in the text and indicated by numbers (see Figure 3d). Grey shading indicates preindustrial CO_2 level of 280 μatm and minimal Pleistocene CO_2 level of 180 μatm . Average error bar is indicated. Records of SST, SSS, ice volume, and $\text{Mg}/\text{Ca}_{\text{s.w.}}$ have been interpolated to fit our time resolution.

negligible, as Mg/Ca_{s,w.} may have increased by 1 mol/mol between 4 and 2.5 Ma [Fantle and DePaolo, 2005, 2006]. Adjusting Mg/Ca-based SST for these secular changes in seawater Mg/Ca contributes to increase Pliocene SST by 3–6°C (4°C on average) at site 999 (Figure 3b). However, it should be noted that these estimates of Mg/Ca_{s,w.} [Fantle and DePaolo, 2005, 2006] have a low temporal resolution and are still controversial, although Coggon *et al.* [2010] also found lower-than-modern Mg/Ca_{s,w.} during the Neogene. Moreover, it is uncertain how the partition coefficient of foraminiferal Mg/Ca is influenced by changes in Mg/Ca_{s,w.} [Medina-Elizalde *et al.*, 2008]. Similar to δ¹¹B_{s,w.}, we calculated seawater pH according to two SST scenarios (1) with unadjusted and (2) with adjusted SST to Mg/Ca_{s,w.}, following Medina-Elizalde *et al.* [2008]. SST were not reconstructed for samples younger than 2.3 Ma by Groeneveld [2005] and an extrapolated temperature of 25.7°C was used to calculate pH and pCO₂ for these four samples.

2.4.4. Uncertainties of Sea Surface Salinity Reconstructions

[17] Local changes in SSS at site 999 (Figure 3c) were estimated using the equation by Steph *et al.* [2006] from seawater δ¹⁸O corrected for changes in global ice volume, where ice volume estimates were taken from Mudelsee and Raymo [2005] (Figure 3c). Seawater δ¹⁸O was calculated following Shackleton [1974] from unadjusted SST and δ¹⁸O measured on *G. sacculifer* [Steph *et al.*, 2009]. For comparison, SSS was also calculated following the same method but using the estimations of sea level changes to correct for changes in global ice volume (Figure S2). Any estimation of Pliocene SSS changes is greatly hindered by the lack of reliable global ice volume or sea level changes for this epoch. However, SSS exerts only a small influence on the uncertainty of pH (±0.01 pH units per ‰ SSS) and of pCO₂. For instance, pCO₂ calculated with a constant salinity of 33.5‰ and of 37.5‰ differ by only 10–20 μatm in comparison.

2.4.5. Uncertainty of Carbonate Ion Concentration Reconstructions

[18] In addition to the pH values derived from δ¹¹B (Figure 3d) a second parameter of the ocean carbonate system is needed to estimate aqueous pCO₂ in seawater. Here we reconstructed the carbonate ion concentration ([CO₃²⁻]) following the method described by Tyrrell and Zeebe [2004], which is based on the observation that the calcite saturation state of seawater (Ω) was quasi-constant over the past 100 My. The calcite saturation state is given by

$$\Omega = [\text{Ca}^{2+}] \times [\text{CO}_3^{2-}] / K_{sp}^*, \quad (2)$$

where K_{sp}^* is the stoichiometric solubility product of calcite. Given the calcium concentration and K_{sp}^* , and assuming Ω approximately constant over the time interval of interest, global ocean [CO₃²⁻] can be calculated back in time [see Tyrrell and Zeebe, 2004]:

$$[\text{CO}_3^{2-}] = \Omega \times K_{sp}^* / [\text{Ca}^{2+}]. \quad (3)$$

[19] In our calculation of carbonate chemistry parameters, we included changes in the ocean's carbonate compensation depth over time [Tyrrell and Zeebe, 2004] and effects of whole ocean [Ca²⁺] and [Mg²⁺] (and the Mg/Ca ratio, [Tyrrell and Zeebe, 2004]) on stoichiometric equilibrium constants K_1^* , K_2^* , and K_{sp}^* [Zeebe and Wolf-Gladrow, 2001]. Effects of local changes in SST and SSS at site 999 (Figures 3b and 3c) on these equilibrium constants were also taken into account for the calculation of [CO₃²⁻] and pCO₂ (Figures 3e and 3f).

[20] In addition, because all parameters are estimated relative to modern conditions, a modern glacial/interglacial average [CO₃²⁻] value is required for site 999. GLODAP data from stations near the core site [Key *et al.*, 2004] indicate a modern (interglacial) CO₃²⁻ concentration of about 290 μmol kg⁻¹. For the last glacial period, [CO₃²⁻] can be estimated as ~340 μmol kg⁻¹, given an atmospheric CO₂ concentration of 200 ppmv. Thus a modern glacial/interglacial average value of [CO₃²⁻] = 315 μmol kg⁻¹ was chosen for site 999 [(290 + 340)/2 = 315], and the global estimates of Tyrrell and Zeebe [2004] were scaled relative to this value. An uncertainty of 1 μmol kg⁻¹ in [CO₃²⁻] translates into an uncertainty of 2 μatm in pCO₂. Finally, given the reconstructed [CO₃²⁻] and pH values, aqueous pCO₂ can be calculated using carbonate chemistry routines as given by Zeebe and Wolf-Gladrow [2001] and Tyrrell and Zeebe [2004]. For comparison, pCO₂ was also estimated using various constant values of [CO₃²⁻] and total alkalinity (Figure S3). However, Pliocene [CO₃²⁻] and total alkalinity were unlikely constant from 1.8 to 4.7 Ma but likely differed from modern values as discussed by Tyrrell and Zeebe [2004].

2.4.6. Propagated Uncertainties

[21] To estimate the contribution of each parameter to the final pH uncertainty, we used an uncertainty of ±1°C (uncertainty on Mg/Ca-derived SST), ±1‰ salinity (because of the uncertainty on ice volume changes), and the analytical uncertainty on δ¹¹B (±0.34‰ on average). The main uncertainty on the pH reconstruction (Table 1) stems from the analytical uncertainty of boron isotope measurements and uncertainties on the SST estimate (±0.04 and ±0.02 pH units, respectively), giving a propagated 2σ uncertainty of ±0.044 pH units on average for all parameters. For estimating uncertainty on our pCO₂ estimates, we estimated a pH uncertainty increasing from -37/+44 μatm at 200 μatm pCO₂ increasing to -73/+88 μatm at 400 μatm pCO₂, and an uncertainty of ±25 μmol kg⁻¹ on [CO₃²⁻]. The average propagated uncertainty on pCO₂ estimates (absolute values) is -70/+80 μatm (Table 1).

3. Age Model

[22] The age model for site 999 was originally established by Haug and Tiedemann [1998] based on benthic foraminiferal δ¹⁸O stratigraphy. Here the benthic δ¹⁸O record from site 999 was correlated to the global stack of 57 benthic foraminiferal δ¹⁸O records (“LR04”) [Lisiecki and Raymo, 2005] without changing the definition of the marine isotope stages (MIS) by Haug and Tiedemann [1998]. The result is displayed in Figure 1. Where it was necessary, SST

Table 1. Averaged Uncertainties on pH and $p\text{CO}_2$ Determination Calculated With $\pm 1^\circ\text{C}$, $\pm 1\%$ salinity, $\pm 0.34\%$ Measured $\delta^{11}\text{B}$, and a $\pm 25 \mu\text{mol kg}^{-1}$ Error on the Carbonate Ion Concentration^a

	SST ($\pm 1^\circ\text{C}$)	SSS ($\pm 1\%$)	$\delta^{11}\text{B}$ ($\pm 0.34\%$) 2 Standard Error on Average)	Propagated Error (Average)
pH with $\delta^{11}\text{B}_{\text{s.w.}}$ = 39.61‰	0.03	0.01	0.08	0.044 pH units
	pH (± 0.044)	$[\text{CO}_3^{2-}]$ ($\pm 25 \mu\text{mol kg}^{-1}$)		
$\Delta p\text{CO}_2$ (μatm)	-53/+66	28		-60/+70 μatm

^aError propagations are the square root of the sum of all squared deviations for each parameter.

and SSS, ice volume, $\text{Mg}/\text{Ca}_{\text{s.w.}}$ and $\delta^{11}\text{B}_{\text{s.w.}}$ were linearly interpolated to fit our time resolution using the AnalySeries 2.0.3 package [Paillard *et al.*, 1996].

4. Results

4.1. Boron Isotope Ratios and Sensitivity Study for pH and $p\text{CO}_2$

[23] Pliocene $\delta^{11}\text{B}$ values ranged between 20.11‰ and 21.70‰ over the time period 4.6–2.0 Ma (Figure 1) and sample preparation did not appear to influence the measured $\delta^{11}\text{B}$ (Data Set S1). For comparison, Pleistocene (2.1–0 Ma) $\delta^{11}\text{B}$ ratios obtained using the same analytical technique but originating from another core site [Hönisch *et al.*, 2009] range between 22.29‰ and 20.55‰ (-1.1% for the offset between laboratories, Figure 4a). Compared to the Pleistocene, the lowest $\delta^{11}\text{B}$ values of the early Pliocene were on average 0.59‰ lower and the highest values were on average 0.65‰ lower, confirming a shift from the early Pliocene toward the Pleistocene following the increase in global ice volume (Figure 4b). The $\delta^{11}\text{B}$ minima-maxima amplitude increased from 0.58‰ during the early Pliocene to 0.94‰ during the late Pliocene, and to 1.1‰ during the early Pleistocene. Between 3.6 and 3.2 Ma, the $\delta^{11}\text{B}$ minima-maxima amplitude was reduced to 0.39‰, and in particular between 3.4 to 3.32 Ma. After 2.7 Ma, the $\delta^{11}\text{B}$ minima-maxima amplitude increased gradually (Figure 4a) toward the Pleistocene amplitudes.

[24] To decipher the uncertainties in $p\text{CO}_2$ linked to uncertainties in $\delta^{11}\text{B}_{\text{s.w.}}$ and $\text{Mg}/\text{Ca}_{\text{s.w.}}$, four scenarios were considered for our pH and $p\text{CO}_2$ estimates (Figures 3d and 3f): Scenario 1 considers unadjusted SST and constant $\delta^{11}\text{B}_{\text{s.w.}}$, scenario 2 considers adjusted SST and constant $\delta^{11}\text{B}_{\text{s.w.}}$, scenario 3 considers unadjusted SST and varying $\delta^{11}\text{B}_{\text{s.w.}}$, and scenario 4 considers adjusted SST and varying $\delta^{11}\text{B}_{\text{s.w.}}$. Adjusting the SST estimate for variations in $\text{Mg}/\text{Ca}_{\text{s.w.}}$ (scenario 2) translates into lowest pH and highest $p\text{CO}_2$ estimates, whereas adjusting for $\delta^{11}\text{B}_{\text{s.w.}}$ (scenario 3) results in the highest pH and lowest $p\text{CO}_2$ estimates. Scenarios 1 (no adjustment) and 4 (adjusting both $\text{Mg}/\text{Ca}_{\text{s.w.}}$ and $\delta^{11}\text{B}_{\text{s.w.}}$) yield very similar results, which are intermediate between scenarios 2 and 3. This may not be surprising as the secular variations in oceanic $\delta^{11}\text{B}_{\text{s.w.}}$ and $\text{Mg}/\text{Ca}_{\text{s.w.}}$ may be coupled via global runoff and weathering as suggested by Paris *et al.* [2010].

[25] The difference in $p\text{CO}_2$ between the four scenarios decreases from 200 μatm at 4.7 Ma to 50 μatm at 2 Ma. Adjusting Mg/Ca -based SST for changes in $\text{Mg}/\text{Ca}_{\text{s.w.}}$ (scenarios 2 and 4) or using a Pliocene value for seawater $\delta^{11}\text{B}_{\text{s.w.}}$ (scenarios 3 and 4) both increase the $p\text{CO}_2$ by 20 to 100 μatm (on average 40–50 μatm). In all scenarios, except scenario 3, early Pliocene $p\text{CO}_2$ estimates are higher than the preindustrial maximum of 280 μatm . Because both models of secular evolution in $\text{Mg}/\text{Ca}_{\text{s.w.}}$ and $\delta^{11}\text{B}_{\text{s.w.}}$ are fraught with uncertainty and because it is unlikely that secular changes occurred only in $\text{Mg}/\text{Ca}_{\text{s.w.}}$ or only in $\delta^{11}\text{B}_{\text{s.w.}}$, we consider the intermediate estimates the best guess at this time. Our further discussions focus on the results of scenario 1.

4.2. Pliocene CO₂ Changes

[26] Calculated aqueous $p\text{CO}_2$ values (scenario 1) at site 999 range between 195 and 425 μatm over the period 4.6–2.0 Ma (Figure 4c and Data Set S1). Small differences exist between the $\delta^{11}\text{B}$ record (Figure 4a) and the calculated $p\text{CO}_2$ record (Figure 4c), however the main trends are the same, confirming that the $p\text{CO}_2$ estimates are not driven by secondary corrections such as SST or $[\text{CO}_3^{2-}]$. The highest $p\text{CO}_2$ values were reached during the early Pliocene prior to 3.6 Ma with a maximum of 425 μatm at 4.58 Ma and 410 μatm on average (Figure 4c). During this period, lowest $p\text{CO}_2$ values ranged 290–330 μatm and 300 μatm on average. Between 3.4 and 3.32 Ma, maximal and minimal $\delta^{11}\text{B}$ values were similar and translated into relatively low $p\text{CO}_2$ values of 290 μatm on average, ranging 250–300 μatm (Figure 4c). During this period, minimal $p\text{CO}_2$ values continued a gradual decrease from $\sim 300 \mu\text{atm}$ to $\sim 245 \mu\text{atm}$ at 3.1 Ma. After 3.1 Ma, maximal $p\text{CO}_2$ values resumed to higher values of $\sim 400 \mu\text{atm}$ ranging 355–420 μatm until 2.7 Ma, when they decreased to $\sim 350 \mu\text{atm}$, still higher by 50 μatm than Pleistocene values. Between 3.1 and 2.7 Ma, minimal (glacial) $p\text{CO}_2$ values were relatively constant at $\sim 245 \mu\text{atm}$. At 2.7 Ma minimal (glacial) $p\text{CO}_2$ abruptly decreased to $\sim 200 \mu\text{atm}$, a level similar to early Pleistocene glacial values (Figure 4c). The $\sim 45/50 \mu\text{atm}$ $p\text{CO}_2$ decrease during glacial stages after 2.7 Ma coincides with a +0.4‰ increase in glacial benthic $\delta^{18}\text{O}$ as reported by Lisiecki and Raymo [2005] (Figure 4b). At 2.2 Ma, maximal CO_2 increased again to 380 μatm and finally decreased to the Pleistocene level of 300 μatm at 2.0 Ma (Figure 4c). During the Pliocene, minima/maxima amplitude of estimated $p\text{CO}_2$ were as high as 100 μatm (Figure 4c), similar to the early Pleistocene [Hönisch *et al.*, 2009].

[27] In summary, our estimates describe a gradual decrease in both minimal and maximal $p\text{CO}_2$ estimates since 4.1 Ma. The total CO_2 decline was $\sim 100 \mu\text{atm}$, with a noted step at 2.7 Ma, when Pleistocene glacial values were reached while interglacial $p\text{CO}_2$ values remained +50 μatm higher than Pleistocene interglacial values until 2.0 Ma (Figure 4c).

5. Discussion

5.1. Comparison With Other CO₂ Records

[28] Because CO_2 is well mixed in the atmosphere and because surface ocean carbonate chemistry at site 999 is close to equilibrium with the atmosphere, we consider our

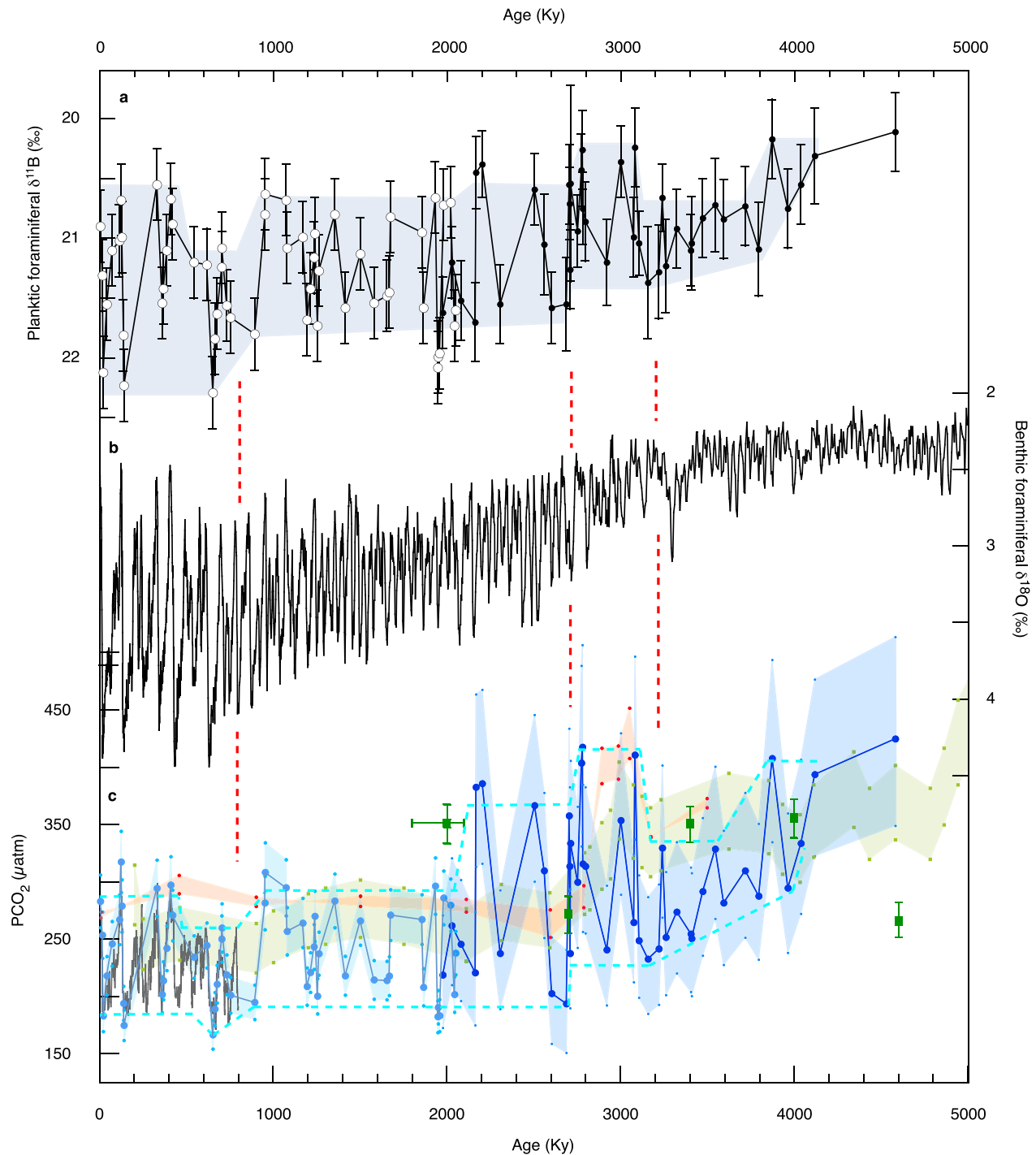


Figure 4. Planktic foraminiferal $\delta^{11}\text{B}$ ratios, benthic $\delta^{18}\text{O}$, and estimated $p\text{CO}_2$ during the Plio-Pleistocene. (a) Planktic foraminiferal $\delta^{11}\text{B}$ ratios measured on *G. sacculifer* (black) with open symbols for the Pleistocene epoch [Hönisch *et al.*, 2009] and with solid symbols for the Pliocene epoch, corrected by -1.1‰ for an offset between the two laboratories (see text) with analytical error bars. (b) Benthic foraminiferal $\delta^{18}\text{O}$ stack LR04 [Lisiecki and Raymo, 2005] reflects changes in deep-sea temperature and ice volume. (c) Atmospheric $p\text{CO}_2$ measured in ice cores [Lüthi *et al.*, 2008] in dark gray, estimated from *G. sacculifer* $\delta^{11}\text{B}$ in light blue [Hönisch *et al.*, 2009] and dark blue (this study) and from *G. ruber* in orange [Seki *et al.*, 2010], estimated from alkenone ε_p in light green squares [Seki *et al.*, 2010] and from stomatal indices in dark green squares [Kürschner *et al.*, 1996]. Upper and lower CO_2 estimates from Seki *et al.* [2010] were obtained by using two different estimations of alkalinity. Red vertical dashed lines denote major climatic transitions: the mid-Pleistocene transition, the late Pliocene transition, and the start of Northern Hemisphere glaciations at 3.3 Ma. The turquoise dashed lines embrace the dominant CO_2 changes as obtained from our boron isotope estimates.

aqueous $p\text{CO}_2$ estimates approximate to atmospheric $p\text{CO}_2$, hereafter referred to as $\delta^{11}\text{B}$ -based $p\text{CO}_2$. At 2.0 Ma our estimates overlap with $p\text{CO}_2$ estimates from the eastern equatorial Atlantic obtained via the same method [Hönisch *et al.*, 2009] (Figure 4), which raises confidence that boron isotope reconstructions from oligotrophic oceanic regions indeed yield reliable estimates of atmospheric $p\text{CO}_2$.

[29] Few stomata index-based CO₂ estimates of 280 and 370 μatm between 3.3 and 2.0 Ma [Kürschner *et al.*, 1996] are also in general agreement with our data (Figure 4c). Pagani *et al.* [2010] reconstructed surface ocean $p\text{CO}_2$ based on alkenone ε_p from 6 locations in the oligotrophic and mesotrophic Atlantic and Pacific Oceans (not shown). For all these locations, their estimates show consistently higher $p\text{CO}_2$ for the Pliocene, although the absolute values differ between sites and only two of their records approach ice core CO₂ values of 170–280 ppmv during the Pleistocene. Pagani *et al.* [2010] estimated average $p\text{CO}_2$ values of 365–415 μatm during the warm early Pliocene, which is similar to our CO₂ estimates (380–420 μatm), and described a decrease of atmospheric $p\text{CO}_2$ by 45–144 μatm or 41–216 μatm , depending on their assumption of nutrient supply, over the last 4.5 Ma. Our boron isotope reconstruction is restricted to the period 4.2–2.0 Ma and registers a relatively similar decrease by 100 μatm .

[30] Pearson and Palmer's [2000] Cenozoic record is also based on planktic foraminiferal $\delta^{11}\text{B}$, using a different analytical technique than in this study. Although their Pliocene estimates show a similar decline in atmospheric CO₂ from 280 to 210 ppm between 3.87 Ma to 3.0 Ma, their low temporal resolution and use of mixed planktic foraminifer species preclude any meaningful comparison. A more detailed comparison can be made with recently published $p\text{CO}_2$ estimates from site 999 based on alkenone ε_p and $\delta^{11}\text{B}$ [Seki *et al.*, 2010]. In general both data sets are in good agreement and show similar CO₂ trends and absolute values through time (Figure 4c). However, the sampling strategy applied by Seki *et al.* [2010] appears to have favored interglacial times, as they did not yield any $p\text{CO}_2$ estimates lower than 250 μatm during the Pleistocene. Similarly, the $p\text{CO}_2$ estimates from alkenone ε_p only reproduce intermediate values (~240 μatm) if low nutrient concentrations are assumed. Their favored scenario of elevated nutrient concentrations agrees well with the boron isotope ratios measured on the same samples but suggests $p\text{CO}_2 > 250 \mu\text{atm}$ for the entire record (Figure 4c).

[31] Finally, reconstructions of Pliocene $p\text{CO}_2$ include estimates from foraminiferal B/Ca ratios (not shown) spanning 3.4–2.4 Ma at western tropical Pacific site 806 [Tripathi *et al.*, 2009]. Their CO₂ data present a maximum for the Pliocene epoch of only 300 μatm ($\pm 50 \mu\text{atm}$) around 3.2 Ma and a decrease to 150 μatm ($\pm 50 \mu\text{atm}$) around 2.8 Ma. This range seems biased toward too low values compared to other Pliocene records, which record atmospheric $p\text{CO}_2$ higher than the preindustrial level for this warm epoch [Seki *et al.*, 2010; Pagani *et al.*, 2010; Kürschner *et al.*, 1996; Raymo *et al.*, 1996], including this present study. Because various calibration data sets for a pH effect on foraminiferal B/Ca ratios show conflicting results [Yu *et al.*, 2007; Foster, 2008; Tripathi *et al.*, 2009], much more information is needed on this new proxy before past $p\text{CO}_2$ reconstructions can be approached with confidence [Tripathi *et al.*, 2011].

[32] With the exception of the B/Ca estimates, all records agree that interglacial Pliocene $p\text{CO}_2$ was higher by about +110 μatm compared to the Pleistocene, although small differences exist in the details of each record. In agreement with studies referenced above, our record shows that a gradual decline in CO₂ by ~100 μatm from 4.1 to 2.0 Ma coincides with the late Pliocene onset and intensification of Northern Hemisphere Glaciations, supporting the link between glaciation and decrease in atmospheric CO₂ concentration, as previously postulated [Raymo *et al.*, 1996; Seki *et al.*, 2010; Pagani *et al.*, 2010] and modeled [Lunt *et al.*, 2008]. However, the higher temporal resolution of this record offers a more detailed perspective on the timing and the supposed causes of the atmospheric CO₂ changes between 2.0 and 3.6 Ma, as described below.

5.2. Implications for the Onset and Intensification of Northern Hemisphere Glaciations

[33] Prior to the start of Northern Hemisphere glaciations, early Pliocene $\delta^{11}\text{B}$ -based $p\text{CO}_2$ values between 4.6 and 3.6 Ma averaged maxima of 410 μatm and minima of 310 μatm , both above a suggested threshold value of 280 μatm below which Northern Hemisphere glaciations are possible [DeConto *et al.*, 2008]. This may explain in part why large-scale glaciations on Greenland were not recorded during this time. Alternatively, Koenig *et al.* [2011] defined other CO₂ threshold values between 200 and 400 μatm for the initiations of glaciations on Greenland by taking into account vegetation changes (i.e., forest versus tundra) over an initially ice-free Greenland. They concluded on a critical role of decreasing atmospheric CO₂ in the glaciation of Greenland at 2.74 Ma, although other albedo-related feedbacks were also significant, including the vegetation cover on Greenland and the sea ice cover in Greenland and Labrador Seas [Koenig *et al.*, 2011]. If the CO₂ threshold defined by Koenig *et al.* [2011] is correct, Miocene and early Pliocene atmospheric CO₂ estimates <400 μatm [Seki *et al.*, 2010; Pagani *et al.*, 2010; Kürschner *et al.*, 1996; this study] would explain why ice-rafted detritus deposition in the North Atlantic could start as early as 5–10 Ma [Wolf and Thiede, 1991; Jansen and Sjøholm, 1991].

[34] After 4.2 Ma and until 2.0 Ma, minima/maxima amplitudes of estimated $p\text{CO}_2$ were as high as 100 μatm (Figure 4c), similar to the Pleistocene glacial/interglacial CO₂ amplitude [Hönisch *et al.*, 2009]. While the Pleistocene amplitude of 100 μatm is still not fully understood [Kohfeld *et al.*, 2005], it is clear that glacial/interglacial CO₂ variations are mainly controlled by the Southern Ocean through ventilation of the deep ocean and biological pump strength [see Sigman *et al.*, 2010]. Although the estimated Pliocene minima/maxima CO₂ amplitudes of 100 μatm require validation by other atmospheric CO₂ records, such amplitudes could be controlled by the state of the Southern Ocean. Indeed, glacial/interglacial oscillations in the size of the West Antarctic Ice Sheet during the early Pliocene [Naish *et al.*, 2009] may have influenced the overturning of the Southern Ocean and the sequestration of atmospheric CO₂ during the early Pliocene. Similarly, it was suggested by Sigman *et al.* [2004] that overturning of the polar oceans could be responsible for large amounts of CO₂ degassing during the late Oligocene and middle Miocene.

[35] After the start of Northern Hemisphere glaciations around 3.6 Ma, maximal $p\text{CO}_2$ estimates transiently decreased from 410 μatm to 260 μatm on average between 3.4 and 3.32 Ma, while minimal $p\text{CO}_2$ estimates gradually decreased from 310 μatm to 245 μatm . A transient increase in glacial and interglacial ice volume is also recorded between 3.43 and 3.32 Ma by an increase of 0.20‰ in the benthic $\delta^{18}\text{O}$ stack LR04 (Figure 4b) and/or by a transient increase of 12 m equivalent sea level (0.11‰ $\delta^{18}\text{O}$) around 3.3 Ma (Figure 3c) [Mudelsee and Raymo, 2005]. The transient glaciation on Greenland at this time also coincides with a transient decrease in North Atlantic SST between 3.3 and 3.5 Ma by 2°C during interglacials and 5°C during glacials at site U1313 [Naafs et al., 2010] and at site 982 [Lawrence et al., 2009]. Increased ice rafted-detritus deposition at 3.3 Ma in the North Atlantic [Jansen et al., 2000; Kleiven et al., 2002] and in the Labrador Sea [Sarnthein et al., 2009] also evidenced the transient increase in the size of the Greenland and Laurentide ice sheets. Although the transient decline in $p\text{CO}_2$ coincides with transient glaciations on Greenland between 3.43 and 3.32 Ma, the maximal $p\text{CO}_2$ estimates between 3.6 and 3.2 Ma are as low as Pleistocene interglacial values, an observation that may be unexpected from comparison with the benthic $\delta^{18}\text{O}$ stack LR04 (Figure 4b). However, several lines of evidence suggest that the low $p\text{CO}_2$ estimates could indicate temporary disequilibrium between surface seawater at site 999 and the atmosphere during this time. Increased nutrient supply to site 999 between 3.5 and 3.1 Ma [Kameo, 2002] and increased surface seawater primary productivity between 3.4 and 3.35 Ma at nearby site 502A [Bornmalm et al., 1999] have been documented for this time, suggesting a possible lowering of surface seawater $p\text{CO}_2$ compared to the atmosphere via increased primary productivity [Wanninkhof et al., 2007]. Similarly, low surface water salinity at site 999 between 3.5 and 3.1 Ma could suggest an inflow of low-salinity and nutrient-rich Amazon and Orinoco river water, brought to the Caribbean Sea by the Guyana Current [Kameo et al., 2004]. In any case, the decrease in $p\text{CO}_2$ estimates appears to have occurred during the start of Northern Hemisphere glaciations at 3.3–3.6 Ma.

[36] Between 3.2 and 2.7 Ma, maximal $p\text{CO}_2$ estimates returned to values of 400 μatm on average until 2.77 Ma (Figure 4c), similar to present-day CO₂ level. Interglacial ice volume also resumed to previous level during this time (Figure 4b). Although it was not the specific focus of this paper, we estimate high $p\text{CO}_2$ of 410 μatm (MIS K1) and 350 μatm (MIS G19) during interglacials of the mid-Pliocene warm period (3.29–2.97 Ma). This confirms the earlier notion that the warmer climate characteristic of the mid-Pliocene warm period may have been partly driven by a stronger greenhouse effect due to higher atmospheric CO₂ [Raymo et al., 1996]. Lunt et al. [2010] discussed in detail the implication of such a result for the estimation of Earth sensitivity through time. Between 3.2 and 2.7 Ma, minimal CO₂ estimates stayed at a level of 245 μatm (Figure 4c), while maximal glacial ice volume also stayed constant between 3.1 and 2.8 Ma, as evidenced by the LR04 benthic $\delta^{18}\text{O}$ stack (Figure 4b). Ice-rafted detritus deposition was also low in the North Atlantic after the transient increase around 3.3 Ma until 2.7 Ma [Kleiven et al., 2002]. Moreover, North Atlantic SST records off South Iceland

increased by 2–3°C during interglacial and glacial stages at site 984 [Bartoli et al., 2005] and site 982 [Lawrence et al., 2009] between 3.05 and 2.80 Ma. This suggests that warming over the northern North Atlantic, associated with high atmospheric CO₂ concentrations and low obliquity [Laskar et al., 2004] jointly prevented the further growth of the Greenland ice sheet between 3.2 and 2.7 Ma.

[37] During the late Pliocene transition at 2.73 Ma, global ice volume increased by 22 m equivalent sea level [Sosdian and Rosenthal, 2009], glacial/interglacial cycles intensified [Lisiecki and Raymo, 2007], deepwater cooled by 2°C [Sosdian and Rosenthal, 2009], and ice-rafted detritus deposition increased over the North Atlantic, thus confirming the increase of the Greenland, Laurentide, and Scandinavian ice sheets [Kleiven et al., 2002]. After 2.7 Ma, our minimal $p\text{CO}_2$ estimates decreased by 45 μatm (Figure 4c) and reached values similar to early Pleistocene glacial values of 200 μatm , while maximal $p\text{CO}_2$ estimates decreased by 50 μatm but stayed +50 μatm higher than during early Pleistocene interglacials. Our results are consistent with the timing of increased stratification in the subarctic North Pacific [Sigman et al., 2004] and in the Southern Ocean [Hodell and Venz-Curtis, 2006; Waddell et al., 2009] at 2.73 Ma. It has been suggested that increased polar stratification led to enhanced sequestration of atmospheric CO₂ in the oceanic abyss after 2.73 Ma, by preventing CO₂-rich deep waters to reach the surface. Stratification thus could have played a major role in the onset of large-scale ice sheets in the Northern Hemisphere [Sigman et al., 2004]. North Pacific stratification alone could account for a decrease of 30–40 μatm [Haug et al., 1999], which is close to the 45 μatm glacial decrease registered in this study between 2.70 and 2.68 Ma. In addition, the strong North Pacific halocline may have persisted during both glacials and interglacial in the North Pacific [Swann, 2010] and thus may have played a role in the 50 μatm decrease during interglacials after 2.7 Ma. Recently, Martínez-García et al. [2011] presented a record of Aeolian iron input to the Southern Ocean that suggests increased iron fertilization during glacials after 2.7 Ma. In addition to polar stratification, increased export production and nutrient utilization in the Southern Ocean thus may have contributed to the glacial decrease in atmospheric CO₂ [Martínez-García et al., 2011]. Increased dust supply to the North Pacific after 2.75 Ma [Bailey et al., 2011] may have had a similar fertilization effect on the North Pacific and adjacent seas, leading to higher CO₂ drawdown in these regions as well. Our results suggest that a threshold was crossed after 2.7 Ma, when the onset of polar stratification and glacial iron fertilization in the North Pacific and Southern Ocean were responsible for the glacial atmospheric CO₂ decrease to values characteristic of Pleistocene glacials. Interestingly, tropical SST changes in various ocean basins show a strong increase in the 41 ky orbital periodicity at 2.7 Ma [Herbert et al., 2010]. This suggests that atmospheric CO₂ and glacial feedbacks after 2.7 Ma were strong enough to imprint a 41 ky periodicity on tropical SST records as compared to prior to 2.7 Ma [Herbert et al., 2010]. Our study agrees well with a decrease in glacial atmospheric CO₂ to Pleistocene levels after 2.7 Ma.

[38] In comparison, maximal $p\text{CO}_2$ estimates decreased by only 50 μatm after 2.7 Ma in our record (Figure 4c) but another high level of 380 μatm is observed at 2.2 Ma,

suggesting that interstadial $p\text{CO}_2$ stayed above early Pleistocene values until 2.0 Ma. A single estimate from stomata also records 360 μatm around 2.0 Ma (Figure 4c). Our findings may suggest that after the sequestration of atmospheric CO₂ in the oceanic abyss after 2.7 Ma, another mechanism was responsible for the lowering interglacial atmospheric CO₂ after 2.2 Ma, such as the intensification of the Benguela upwelling system between 2.1 and 1.9 Ma, which would have increased the efficiency of the biological pump [Marlow *et al.*, 2000]. Alternatively, Etourneau *et al.* [2010] suggested that increased upwelling off Namibia between 2.4 and 2.0 Ma would have increased atmospheric CO₂ by releasing deep water CO₂ to the surface and thereby counteracting the effects of atmospheric CO₂ sequestration elsewhere in the oceans until 2.0 Ma. This mechanism is also supported by our data showing increased atmospheric CO₂ at 2.2 Ma compared to 2.5 Ma.

[39] In summary, the increase in the size of the Greenland ice sheet during the Pliocene epoch was short lived between 3.43 and 3.32 Ma [Lisiecki and Raymo, 2005] and permanent after 2.7 Ma [Haug *et al.*, 2005], and is matched by decreased atmospheric CO₂ concentrations as compared to the early Pliocene. Following the pattern given by the LR04 benthic $\delta^{18}\text{O}$ stack (Figure 4b) and tropical SSTs [Herbert *et al.*, 2010, Figure 6], minimal atmospheric CO₂ concentrations decreased faster than maximal atmospheric CO₂ concentrations over the course of the Plio-Pleistocene. It seems that an important climatic threshold was crossed at 2.7 Ma, when estimated $p\text{CO}_2$ minima decreased by $\sim 45 \mu\text{atm}$ and approached early Pleistocene glacial values. This decrease and its timing are consistent with the onset of polar stratification [Haug *et al.*, 1999; Sigman *et al.*, 2004] associated with iron fertilization in the Southern Ocean [Martinez-Garcia *et al.*, 2011] and in the North Pacific [Bailey *et al.*, 2011]. It is possible that Southern Ocean stratification starting around 3.3 Ma [Hillenbrand and Cortese, 2006] has contributed to the early atmospheric CO₂ decrease between 3.43 and 3.32 Ma, although the role of terrestrial weathering, in particular of the Tibetan-Himalayan Plateau between 4.2 and 2.7 Ma [Zhang *et al.*, 2009], and other possible mechanisms also have to be considered. Based on the timing of the precursor and final closures of Panama dated at 3.15–3.3 Ma and at 2.82–2.95 Ma [Bartoli *et al.*, 2005], the final closure of Panama did not influence the decrease in atmospheric CO₂ recorded here. It can be postulated that a decrease in atmospheric CO₂ concentrations was necessary in order to sustain large-scale glaciations in the Northern Hemisphere after 2.7 Ma, as opposed to the ephemeral glaciations of the Pliocene prior to 3.2 Ma.

6. Conclusions

[40] We reconstructed Pliocene atmospheric CO₂ based on foraminiferal $\delta^{11}\text{B}$ between 4.6 and 2.0 Ma. Our data contribute to previously published evidence that suggests atmospheric CO₂ was higher during the Pliocene epoch by 130 μatm compared to preindustrial levels, and close to the modern level of 400 μatm . Estimated $p\text{CO}_2$ decreased during both the start and the intensification of Northern Hemisphere glaciations around 3.3 Ma and at 2.7 Ma, respectively. After 2.7 Ma, minimal atmospheric CO₂ dropped to values characteristic of early Pleistocene glacials,

consistent with the suggested increased sequestration of atmospheric CO₂ in the North Pacific and Southern Ocean via polar stratification and increased iron fertilization. In comparison, maximal CO₂ estimates reached Pleistocene values only after 2.0 Ma and stayed below 300 μatm until the 1940s.

[41] **Acknowledgments.** We thank the Ocean Drilling Program for making the samples available for this study and M. Schmidt for sharing some of his samples. S. Bernasconi and T. Schmid are acknowledged for providing stable isotopes analyses, U. Brupbacher for laboratory assistance, and M. Medina-Elizalde for helping us with the adjustment of Mg/Ca-based temperatures. Discussions with G. Haug, S. Jaccard, and A. Martinez-Garcia were extremely useful. One anonymous reviewer, G. L. Foster, and the editor C. Charles are thanked for comments that helped improve this manuscript. This work was supported by Swiss National Foundation grant 200020-118045/1 and Individual short visit grant NF P1012-119420 (G.B.), by NSF OCE 06-23621 (B.H.), and by NSF OCE09-27089 (R.E.Z.). B.H. also thanks G. Lenfest for providing the funds for the TRITON at LDEO.

References

- Bailey, I., Q. Liu, G. E. A. Swann, Z. Jiang, Y. Sun, X. Zhao, and A. P. Roberts (2011), Iron fertilisation and biogeochemical cycles in the sub-Arctic northwest Pacific during the late Pliocene intensification of Northern Hemisphere glaciation, *Earth Planet. Sci. Lett.*, 307(3–4), 253–265, doi:10.1016/j.epsl.2011.05.029.
- Ballantyne, A. P., et al. (2006), Pliocene Arctic temperature constraints from the growth rings and isotopic composition of fossil larch, *Palaeogeogr. Palaeoclim. Palaeoecol.*, 242, 188–200, doi:10.1016/j.palaeo.2006.05.016.
- Bartoli, G., M. Sarnthein, M. Weinelt, H. Erlenkeuser, D. Garbe-Schönberg, and D. Lea (2005), Final closure of Panama and the onset of Northern Hemisphere glaciation, *Earth Planet. Sci. Lett.*, 237, 33–44, doi:10.1016/j.epsl.2005.06.020.
- Borrmalm, L., et al. (1999), Changes in circulation and trophic levels in the Pliocene Caribbean Sea: Evidence from benthic foraminifer accumulation rates, *J. Foraminiferal Res.*, 29(3), 209–221.
- Coggon, R. M., D. A. H. Teagle, C. E. Smith-Duque, J. C. Alt, and M. J. Cooper (2010), Reconstructing past seawater Mg/Ca and Sr/Ca from mid-ocean ridge flank calcium carbonate veins, *Science*, 327(5969), 1114–1117, doi:10.1126/science.1182252.
- DeConto, R. M., et al. (2008), Thresholds for Cenozoic bipolar glaciation, *Nature*, 455, 652–656, doi:10.1038/nature07337.
- Delaney, M. L., et al. (1985), Li, Sr, Mg and Na in foraminiferal calcite shells from laboratory culture, sediment traps, and sediment cores, *Geochim. Cosmochim. Acta*, 49, 1327–1341, doi:10.1016/0016-7037(85)90284-4.
- Deyhle, A., and A. Kopf (2004), Possible influence of clay contamination on B isotope geochemistry of carbonaceous samples, *Appl. Geochem.*, 19(5), 737–745, doi:10.1016/j.apgeochem.2003.10.008.
- Dickson, A. G. (1990), Thermodynamics of the dissociation of boric acid in synthetic seawater from 273.15 to 318.15 K, *Deep Sea Res., Part I*, 37, 755–766, doi:10.1016/0198-0149(90)90004-F.
- Etourneau, J., R. Schneider, T. Blanz, and P. Martinez (2010), Intensification of the Walker and Hadley atmospheric circulations during the Pliocene-Pleistocene climate transition, *Earth Planet. Sci. Lett.*, 297(1–2), 103–110, doi:10.1016/j.epsl.2010.06.010.
- Fantle, M. S., and D. J. DePaolo (2005), Variations in the marine Ca cycle over the past 20 million years, *Earth Planet. Sci. Lett.*, 237, 102–107, doi:10.1016/j.epsl.2005.06.024.
- Fantle, M. S., and D. J. DePaolo (2006), Sr isotopes and pore fluid chemistry in carbonate sediment of the Ontong Java Plateau: Calcite recrystallization rates and evidence for a rapid rise in seawater Mg over the last 10 million years, *Geochim. Cosmochim. Acta*, 70, 3883–3904, doi:10.1016/j.gca.2006.06.009.
- Foster, G. L. (2008), Seawater pH, $p\text{CO}_2$ and $[\text{CO}_3^{2-}]$ variations in the Caribbean Sea over the last 130 kyr: A boron isotope and B/Ca study of planktic foraminifera, *Earth Planet. Sci. Lett.*, 271(1–4), 254–266, doi:10.1016/j.epsl.2008.04.015.
- Foster, G. L., P. A. E. Pogge von Strandmann, and J. W. B. Rae (2010), Boron and magnesium isotopic composition of seawater, *Geochem. Geophys. Geosyst.*, 11, Q08015, doi:10.1029/2010GC003201.
- Groeneveld, J. (2005), Effect of the Pliocene closure of the Panamanian Gateway on Caribbean and east Pacific sea surface temperatures and

- salinities by applying combined Mg/Ca and 18O measurements (5.6–2.2 Ma), Ph.D. thesis, 161 pp., Univ. of Kiel, Kiel, Germany.
- Haug, G. H., and R. Tiedemann (1998), Effect of the formation of the Isthmus of Panama on Atlantic Ocean thermohaline circulation, *Nature*, *393*, 673–676, doi:10.1038/31447.
- Haug, G. H., D. M. Sigman, R. Tiedemann, T. F. Pedersen, and M. Samthein (1999), Onset of permanent stratification in the subarctic Pacific Ocean, *Nature*, *401*, 779–782, doi:10.1038/44550.
- Haug, G. H., et al. (2001), Role of Panama uplift on oceanic freshwater balance, *Geology*, *29*(3), 207–210, doi:10.1130/0091-7613(2001)029<0207:ROPUOO>2.0.CO;2.
- Haug, G. H., et al. (2005), North Pacific seasonality and the glaciation of North America 2.7 million years ago, *Nature*, *433*, 821–825, doi:10.1038/nature03332.
- Haywood, A. M., and P. J. Valdes (2004), Modelling Pliocene warmth: Contribution of atmosphere, oceans, and cryosphere, *Earth Planet. Sci. Lett.*, *218*, 363–377, doi:10.1016/S0012-821X(03)00685-X.
- Hemming, N. G., and G. N. Hanson (1992), Boron isotopic composition and concentration in modern marine carbonates, *Geochim. Cosmochim. Acta*, *56*(1), 537–543, doi:10.1016/0016-7037(92)90151-8.
- Herbert, T. D., et al. (2010), Tropical ocean temperatures over the past 3.5 million years, *Science*, *328*(5985), 1530–1534, doi:10.1126/science.1185435.
- Hillenbrand, C.-D., and G. Cortese (2006), Polar stratification: A critical view from Southern Ocean, *Palaeogeogr. Palaeoclimatol. Palaeoecol.*, *242*, 240–252, doi:10.1016/j.palaeo.2006.06.001.
- Hodell, D. A., and K. A. Venz-Curtis (2006), Late Neogene history of deepwater ventilation in the Southern Ocean, *Geochem. Geophys. Geosyst.*, *7*, Q09001, doi:10.1029/2005GC001211.
- Hönisch, B., and N. G. Hemming (2004), Ground-truthing the boron isotope-paleo-pH proxy in planktonic foraminifera shells: Partial dissolution and shell size effects, *Paleoceanography*, *19*, PA4010, doi:10.1029/2004PA001026.
- Hönisch, B., and N. G. Hemming (2005), Surface ocean pH response to variations in pCO₂ through two full glacial cycles, *Earth Planet. Sci. Lett.*, *236*, 305–314, doi:10.1016/j.epsl.2005.04.027.
- Hönisch, B., et al. (2007), Comment on “A critical evaluation of the boron isotope-pH proxy: The accuracy of ancient ocean pH estimates” by M. Pagani, D. Lemarchand, A. Spivack and J. Gaillardet, *Geochim. Cosmochim. Acta*, *71*(6), 1636–1641, doi:10.1016/j.gca.2006.07.045.
- Hönisch, B., et al. (2009), Atmospheric carbon dioxide concentration across the mid-Pleistocene transition, *Science*, *324*(5934), 1551–1554, doi:10.1126/science.1171477.
- Huybers, P., and P. Molnar (2007), Tropical cooling and the onset of North American glaciation, *Clim. Past Discuss.*, *3*, 549–557, doi:10.5194/cp-3-549-2007.
- Jansen, E., and J. Sjøholm (1991), Reconstruction of glaciation over the past 6 Myr from ice-borne deposits in the Norwegian Sea, *Nature*, *349*, 600–603, doi:10.1038/349600a0.
- Jansen, E., T. Fronval, F. Rack, and J. E. T. Channell (2000), Pliocene-Pleistocene ice rafting history and cyclicity in the Nordic Seas during the last 3.5 Myr, *Paleoceanography*, *15*(6), 709–721, doi:10.1029/1999PA000435.
- Kameo, K. (2002), Late Pliocene Caribbean surface water dynamics and climatic changes based on calcareous nannofossil records, *Palaeogeogr. Palaeoclimatol. Palaeoecol.*, *179*(3–4), 211–226, doi:10.1016/S0031-0182(01)00432-1.
- Kameo, K., M. C. Shearer, A. W. Droxler, I. Mita, R. Watanabe, and T. Sato (2004), Glacial-interglacial surface water variations in the Caribbean Sea during the last 300 ky based on calcareous nannofossil analysis, *Palaeogeogr. Palaeoclimatol. Palaeoecol.*, *212*(1–2), 65–76, doi:10.1016/j.palaeo.2004.05.017.
- Key, R. M., A. Kozyr, C. L. Sabine, K. Lee, R. Wanninkhof, J. L. Bullister, R. A. Feely, F. J. Millero, C. Mordy, and T.-H. Peng (2004), A global ocean carbon climatology: Results from Global Data Analysis Project (GLODAP), *Global Biogeochem. Cycles*, *18*, GB4031, doi:10.1029/2004GB002247.
- Kleiven, H. F., E. Jansen, T. Fronval, and T. M. Smith (2002), Intensification of Northern Hemisphere glaciations in the circum Atlantic region (3.5–2.4 Ma)—Ice-rafted detritus evidence, *Palaeogeogr. Palaeoclimatol. Palaeoecol.*, *184*, 213–223, doi:10.1016/S0031-0182(01)00407-2.
- Klochko, K., et al. (2006), Experimental measurement of boron isotope fractionation in seawater, *Earth Planet. Sci. Lett.*, *248*(1–2), 276–285, doi:10.1016/j.epsl.2006.05.034.
- Koenig, S., R. DeConto, and D. Pollard (2011), Late Pliocene to Pleistocene sensitivity of the Greenland Ice Sheet in response to external forcing and internal feedbacks, *Clim. Dyn.*, *37*, 1247–1268, doi:10.1007/s00382-011-1050-0.
- Kohfeld, K. E., C. L. Quéré, S. P. Harrison, and R. F. Anderson (2005), Role of marine biology in glacial-interglacial CO₂ cycles, *Science*, *308*(5718), 74–78, doi:10.1126/science.1105375.
- Kürschner, W. M., et al. (1996), Oak leaves as biosensors of late Neogene and early Pleistocene paleoatmospheric CO₂ concentrations, *Mar. Micro-paleontol.*, *27*, 299–312, doi:10.1016/0377-8398(95)00067-4.
- Laskar, J., P. Robutel, F. Joutel, M. Gastineau, A. C. M. Correia, and B. Levrard (2004), A long-term numerical solution for the insolation quantities of the Earth, *Astron. Astrophys.*, *428*(1), 261–285, doi:10.1051/0004-6361:20041335.
- Lawrence, K. T., T. D. Herbert, C. M. Brown, M. E. Raymo, and A. M. Haywood (2009), High-amplitude variations in North Atlantic sea surface temperature during the early Pliocene warm period, *Paleoceanography*, *24*, PA2218, doi:10.1029/2008PA001669.
- Lemarchand, D., et al. (2000), The influence of rivers on marine boron isotopes and implications for reconstructing past ocean pH, *Nature*, *408*, 951–954, doi:10.1038/35050058.
- Lemarchand, D., et al. (2002), Boron isotope systematics in large rivers: Implications for the marine boron budget and paleo-pH reconstruction over the Cenozoic, *Chem. Geol.*, *190*(1–4), 123–140, doi:10.1016/S0009-2541(02)00114-6.
- Li, X. S., A. Berger, M. F. Loutre, M. A. Maslin, G. H. Haug, and R. Tiedemann (1998), Simulating late Pliocene Northern Hemisphere climate with the LLN 2-D model, *Geophys. Res. Lett.*, *25*(6), 915–918, doi:10.1029/98GL00443.
- Lisiecki, L. E., and M. E. Raymo (2005), A Pliocene-Pleistocene stack of 57 globally distributed benthic δ¹⁸O records, *Paleoceanography*, *20*, PA1003, doi:10.1029/2004PA001071.
- Lisiecki, L. E., and M. E. Raymo (2007), Plio-Pleistocene climate evolution: Trends and transitions in glacial cycle dynamics, *Quat. Sci. Rev.*, *26*, 56–69, doi:10.1016/j.quascirev.2006.09.005.
- Lunt, D. J., et al. (2008), Late Pliocene Greenland glaciation controlled by a decline in atmospheric CO₂ levels, *Nature*, *454*, 1102–1105, doi:10.1038/nature07223.
- Lunt, D. J., et al. (2010), Earth system sensitivity inferred from Pliocene modelling and data, *Nat. Geosci.*, *3*(1), 60–64, doi:10.1038/ngeo706.
- Lüthi, D., et al. (2008), High-resolution carbon dioxide concentration record 650,000–800,000 years before present, *Nature*, *453*(7193), 379–382, doi:10.1038/nature06949.
- Marlow, J. R., et al. (2000), Upwelling intensification as part of the Pliocene-Pleistocene climate transition, *Science*, *290*, 2288–2291, doi:10.1126/science.290.5500.2288.
- Martin, P. A., and D. W. Lea (2002), A simple evaluation of cleaning procedures on fossil benthic foraminiferal Mg/Ca, *Geochem. Geophys. Geosyst.*, *3*(10), 8401, doi:10.1029/2001GC000280.
- Martínez-García, A., et al. (2011), Southern Ocean dust-climate coupling over the last four million years, *Nature*, *476*, 312–315, doi:10.1038/nature10310.
- Medina-Elizalde, M., et al. (2008), Implications of seawater Mg/Ca variability for Plio-Pleistocene tropical climate reconstruction, *Earth Planet. Sci. Lett.*, *269*(3–4), 585–595, doi:10.1016/j.epsl.2008.03.014.
- Mudelsee, M., and M. E. Raymo (2005), Slow dynamics of the Northern Hemisphere glaciation, *Paleoceanography*, *20*, PA4022, doi:10.1029/2005PA001153.
- Naafs, B. D. A., R. Stein, J. Hefter, N. Khélifi, S. De Schepper, and G. H. Haug (2010), Late Pliocene changes in the North Atlantic Current, *Earth Planet. Sci. Lett.*, *298*(3–4), 434–442, doi:10.1016/j.epsl.2010.08.023.
- Naish, T., et al. (2009), Obliquity-paced Pliocene West Antarctic ice sheet oscillations, *Nature*, *458*(7236), 322–328, doi:10.1038/nature07867.
- Ni, Y., G. L. Foster, T. Bailey, T. Elliott, D. N. Schmidt, P. Pearson, B. Haley, and C. Coath (2007), A core top assessment of proxies for the ocean carbonate system in surface-dwelling foraminifers, *Paleoceanography*, *22*, PA3212, doi:10.1029/2006PA001337.
- O’Dea, A., et al. (2007), Environmental change preceded Caribbean extinction by 2 million years, *Proc. Natl. Acad. Sci. U. S. A.*, *104*(13), 5501–5506, doi:10.1073/pnas.0610947104.
- Pagani, M., et al. (2010), High Earth-system climate sensitivity determined from Pliocene carbon dioxide concentrations, *Nat. Geosci.*, *3*(1), 27–30, doi:10.1038/ngeo724.
- Paillard, D., L. Labeyrie, and P. Yiou (1996), Macintosh program performs time-series analysis, *Eos Trans. AGU*, *77*, 379, doi:10.1029/96EO00259.
- Paris, G., J. Gaillardet, and P. Louvat (2010), Geological evolution of seawater boron isotopic composition recorded in evaporates, *Geology*, *38*(11), 1035–1038, doi:10.1130/G31321.1.
- Pearson, P. N., and M. R. Palmer (1999), Middle Eocene seawater pH and atmospheric carbon dioxide concentrations, *Science*, *284*, 1824–1826, doi:10.1126/science.284.5421.1824.

- Pearson, P. N., and M. R. Palmer (2000), Atmospheric carbon dioxide concentrations over the past 60 millions years, *Nature*, *406*, 695–699, doi:10.1038/35021000.
- Raymo, M. E., et al. (1996), Mid-Pliocene warmth: Stronger greenhouse and stronger conveyor, *Mar. Micropaleontol.*, *27*, 313–326, doi:10.1016/0377-8398(95)00048-8.
- Sanyal, A., J. Bijma, H. Spero, and D. W. Lea (2001), Empirical relationship between pH and the boron isotopic composition of *Globigerinoides sacculifer*: Implications for the boron isotope paleo-pH proxy, *Paleoceanography*, *16*(5), 515–519, doi:10.1029/2000PA000547.
- Sarnthein, M., et al. (2009), Mid-Pliocene shifts in ocean overturning circulation and the onset of Quaternary-style climates, *Clim. Past*, *5*(2), 269–283, doi:10.5194/cp-5-269-2009.
- Seki, O., et al. (2010), Alkenone and boron-based Pliocene pCO₂ records, *Earth Planet. Sci. Lett.*, *292*(1–2), 201–211, doi:10.1016/j.epsl.2010.01.037.
- Shackleton, N. J. (1974), Attainment of isotopic equilibrium between ocean water and the benthonic foraminifera genus *Uvigerina*: Isotopic changes in the ocean during the last glacial, *Colloq. Int. C. N. R. S.*, *219*, 203–209.
- Sigman, D. M., et al. (2004), Polar ocean stratification in a cold climate, *Nature*, *428*, 59–63, doi:10.1038/nature02357.
- Sigman, D. M., et al. (2010), The polar ocean and glacial cycles in atmospheric CO₂ concentration, *Nature*, *466*(7302), 47–55, doi:10.1038/nature09149.
- Simon, L., et al. (2006), Modelling the geochemical cycle of boron: Implications for the long-term δ¹¹B evolution of seawater and oceanic crust, *Chem. Geol.*, *225*, 61–76, doi:10.1016/j.chemgeo.2005.08.011.
- Sosdian, S., and Y. Rosenthal (2009), Deep-sea temperature and ice volume changes across the Pliocene-Pleistocene climate transitions, *Science*, *325*(5938), 306–310, doi:10.1126/science.1169938.
- Spivack, A. J., and J. M. Edmond (1987), Boron isotope exchange between seawater and the oceanic crust, *Geochim. Cosmochim. Acta*, *51*(5), 1033–1043.
- Steph, S., R. Tiedemann, M. Prange, J. Groeneveld, D. Nürnberg, L. Reuning, M. Schulz, and G. H. Huang (2006), Changes in Caribbean surface hydrography during the Pliocene shoaling of the Central American Seaway, *Paleoceanography*, *21*, PA4221, doi:10.1029/2004PA001092.
- Steph, S., et al. (2009), Stable isotopes of planktonic foraminifera from tropical Atlantic/Caribbean core-tops: Implications for reconstructing upper ocean stratification, *Mar. Micropaleontol.*, *71*(1–2), 1–19, doi:10.1016/j.marmicro.2008.12.004.
- Steph, S., R. Tiedemann, M. Prange, J. Groeneveld, M. Schulz, A. Timmermann, D. Nürnberg, C. Rühlemann, C. Saukel, and G. H. Huang (2010), Early Pliocene increase in thermohaline overturning: A precondition for the development of the modern equatorial Pacific cold tongue, *Paleoceanography*, *25*, PA2202, doi:10.1029/2008PA001645.
- Swann, G. E. A. (2010), Salinity changes in the north west Pacific Ocean during the late Pliocene/early Quaternary from 2.73 Ma to 2.52 Ma, *Earth Planet. Sci. Lett.*, *297*, 332–338, doi:10.1016/j.epsl.2010.06.035.
- Takahashi, T., S. C. Sutherland, and A. Kozyr (2007), Global Ocean Surface Water Partial Pressure of CO₂ Database: Measurements Performed During 1968–2007 (Version 2007), http://cdiac.ornl.gov/oceans/ndp_088/index.html, Oak Ridge Natl. Lab., Oak Ridge, Tenn.
- Tripati, A. K., et al. (2009), Coupling of CO₂ and ice sheet stability over major climate transitions of the last 20 million years, *Science*, *326*(5958), 1394–1397, doi:10.1126/science.1178296.
- Tripati, A. K., et al. (2011), A 20 million year record of planktic foraminiferal B/Ca ratios: Systematics and uncertainties in pCO₂ reconstructions, *Geochim. Cosmochim. Acta*, *75*(10), 2582–2610, doi:10.1016/j.gca.2011.01.018.
- Tyrrell, T., and R. E. Zeebe (2004), History of carbonate ion concentration over the last 100 million years, *Geochim. Cosmochim. Acta*, *68*(17), 3521–3530, doi:10.1016/j.gca.2004.02.018.
- Vizcaíno, M., S. Rupper, and J. C. H. Chiang (2010), Permanent El Niño and the onset of Northern Hemisphere glaciations: Mechanism and comparison with other hypotheses, *Paleoceanography*, *25*, PA2205, doi:10.1029/2009PA001733.
- Waddell, L. M., I. L. Hendy, T. C. Moore, and M. W. Lyle (2009), Ventilation of the abyssal Southern Ocean during the late Neogene: A new perspective from the subantarctic Pacific, *Paleoceanography*, *24*, PA3206, doi:10.1029/2008PA001661.
- Wanninkhof, R., et al. (2007), Air-sea CO₂ fluxes in the Caribbean Sea from 2002–2004, *J. Mar. Syst.*, *66*, 272–284, doi:10.1016/j.jmarsys.2005.11.014.
- Wolf, T. C. W., and J. Thiede (1991), History of terrigenous sedimentation during the past 10 m.y. in the North Atlantic (ODP Legs 104 and 105 and DSDP Leg 81), *Mar. Geol.*, *101*(1–4), 83–102, doi:10.1016/0025-3227(91)90064-B.
- Yu, J., H. Elderfield, and B. Hönisch (2007), B/Ca in planktonic foraminifera as a proxy for surface seawater pH, *Paleoceanography*, *22*, PA2202, doi:10.1029/2006PA001347.
- Zeebe, R. E., and D. A. Wolf-Gladrow (2001), *CO₂ in Seawater: Equilibrium, Kinetics, Isotopes*, Elsevier Oceanogr. Ser., *65*, 346 pp.
- Zhang, Y. G., et al. (2009), Mid-Pliocene Asian monsoon intensification and the onset of Northern Hemisphere glaciation, *Geology*, *37*(7), 599–602, doi:10.1130/G25670A.1.

G. Bartoli, Geological Institute, ETH Zürich, Sonneggstr. 5, CH-8092 Zürich, Switzerland. (gretta.bartoli@erdw.ethz.ch)

B. Hönisch, Lamont-Doherty Earth Observatory, Earth Institute at Columbia University, 61 Route 9W, Palisades, NY 10964, USA.

R. E. Zeebe, Department of Oceanography, School of Ocean and Earth Science and Technology, University of Hawai'i at Mānoa, 1000 Pope Rd., MSB 504, Honolulu, HI 96822, USA.